Climate change-driven coastal flooding in the Mid Adriatic Sea and adaptation of coastal defense structures

Article *in* Estuarine Coastal and Shelf Science · November 2025

DOI: 10.1016/j.ecss.2025.109535

CITATIONS
0

READS
20

5 authors, including:

Agnese Baldoni
Marche Polytechnic University
10 PUBLICATIONS **40** CITATIONS
SEE PROFILE

Francesco Marini
Marche Polytechnic University
18 PUBLICATIONS **97** CITATIONS
SEE PROFILE

Maurizio Brocchini
Marche Polytechnic University
286 PUBLICATIONS **5,691** CITATIONS
SEE PROFILE

Estuarine, Coastal and Shelf Science 326 (2025) 109535

Contents lists available at ScienceDirect

Estuarine, Coastal and Shelf Science

journal homepage: www.elsevier.com/locate/ecss

Climate change-driven coastal flooding in the Mid Adriatic Sea and adaptation of coastal defense structures☆

Agnese Baldoni [a], Francesco Marini [a,*], Giorgio Filomena [b], Stefano Parlani [b], Maurizio Brocchini [a]

[a] Università Politecnica delle Marche, Department of Construction, Civil Engineering and Architecture (DICEA), Via Brecce Bianche 12, Ancona, 60131, AN, Italy
[b] Dipartimento Infrastrutture, Territorio e Protezione Civile, Regione Marche, Ancona, Italy

ARTICLE INFO

Dataset link: A simple code for shoreline recession (Original data)

Keywords:
Coastal flooding
Adriatic sea
Climate change adaptation
Coastal defense structures
Bivariate analysis

ABSTRACT

The Adriatic Sea is highly impacted by rising sea levels and increasingly frequent extreme events due to climate change consequences. This work aims at evaluating coastal flooding caused by future extreme sea storms for five test sites along the Marche Region coast (Italy). Projections of water levels and waves to 2070, under the very high emission scenario identified by the IPCC, were used to force a modeling chain that provided the inundation extent and the water depths in the flooded areas. To define the joint probability of wave height and period, accounting for their mutual dependence, a bivariate extreme value analysis was performed. An extreme pair of wave height-peak period was computed through a copula approach that better allows to understand the correlation between wave energy and storm dynamics compared to univariate methods. Regardless of the analyzed site, coastal flooding affects all the beaches and summer facilities and extends hundred of meters inland, interesting also urban areas and strategic infrastructures. The extension of the flooding increases with increasing return periods, showing the consequences of medium-to-low probability extreme events, projected to occur once in a year by the end of the century. To face such situation, coastal defense structures need to be adapted, carefully selecting the best adaptation option to undertake. While for emerged breakwaters increasing their height always results in a reduced flooding, for submerged barriers a negative effect occurs when the freeboard approaches zero: even if the wave transmission is reduced, a large piling-up generates in the protected area, enlarging the inundation extent, as shown by numerical results.

1. Introduction

Coastal regions are strongly exposed to the impacts of climate change (CC) due to the high population density, the presence of urban centers and infrastructures and the concentration of economic and recreational activities. Sea level rise (SLR) is projected to increase even under the most optimistic emission scenario identified by the Intergovernmental Panel on Climate Change (IPCC) (IPCC, 2023). This, coupled with storm surges and tides, will generate extreme sea level events causing flooding and damages to coastal infrastructures, but also losses of coastal ecosystems and biodiversity and groundwater salinization. By 2050, one billion people will be exposed to extreme sea level events, with 100-years return period events becoming 20–30 times more frequent (IPCC, 2023). CC will also induce changes in ocean wave climate, and especially in extremes, that will combine with those mentioned above, worsening the flooding hazard for coastal settlements and impacting the maritime activities.

Giorgi (2006) identified the Mediterranean region as one of the most sensitive and responsive areas to CC. Due to its prominent role in the development of human culture and economy and the high urbanization of its littoral zone, it becomes of foremost importance understanding and monitoring oceanographic variables, such as waves and water levels, and their impacts. Within the Mediterranean basin, the Adriatic Sea is a semi-enclosed basin highly impacted by variations in mean sea level (Lionello et al., 2017). The interest for this area is highlighted by several studies on future trends of both water levels (Vilibić et al., 2017; Valle-Levinson et al., 2021) and storminess (Bonaldo et al., 2017, 2020).

Awareness of CC-related hazards is increasing among the population and decision makers, this generating an increased emphasis on climate risk assessment and adaptation strategies within the planning and management policies (Bonaldo et al., 2019). In the last decade, the European Union has funded several projects focused on the development

☆ This article is part of a Special issue entitled: 'The Adriatic blue growth' published in Estuarine, Coastal and Shelf Science.

* Corresponding author.
E-mail address: f.marini@staff.univpm.it (F. Marini).

https://doi.org/10.1016/j.ecss.2025.109535
Received 18 March 2025; Accepted 8 September 2025
Available online 14 September 2025

of innovative approaches to define coastal vulnerability, favoring collaboration among different countries, and research and administration institutions. An example are the Italy-Croatia Cross-Border-Cooperation Programs, aimed at improving the life quality of citizens living in the Adriatic area through the exchange of knowledge and experiences among stakeholders, the implementation of pilot action products and services, and the testing of new policies.

Within this framework, the Marche Region, one of the 20 administrative divisions of Italy, facing the Mid Adriatic Sea, adopted its Integrated Coastal Zone Management (ICZM) Plan in 2019 (Regione Marche, 2019). The Plan identifies risks for coastal areas and programs maintenance operations and interventions for coastal defenses, together with a monitoring plan to verify the effectiveness of the planned actions. Furthermore, the Marche Region in collaboration with a consortium of research institutes, drafted its Regional Plan for Adaptation to Climate Change that, based on the scientific analysis on inundation boundaries (Baldoni et al., 2024), has assessed the main vulnerabilities of coastal systems, following an impact chain approach (Zebisch et al., 2022).

This work, funded under the "CoAStal and marine waters integrated monitoring systems for ecosystems proteCtion AnD managemEnt" Interreg Italy-Croatia CASCADE project (2020–2023), represents a fruitful collaboration between the Marche Region and the Università Politecnica delle Marche aimed to perform a step forward in the evaluation of inundation perimeters for five vulnerable sites along the Adriatic coast. Some of the test cases are estuarine locations, others host harbor facilities and/or coastal defense structures. Furthermore, they are characterized by different sediment types, either sand or gravel. To gain detailed knowledge on the flooding extent expected under a severe CC scenario, we used a model chain approach similar to that used in Baldoni et al. (2024), which has shown better performances than the simplistic "bathtub" method when it comes to define site-specific flood mapping and adaptation measures to be undertaken. Being a static model, the "bathtub" approach identifies flooded areas as those whose elevation is below the maximum water surface elevation. Because of its ease of application even over large scales, only requiring a Digital Elevation Model (DEM) and shoreline water level as inputs, such method is the most commonly used for assessing flood hazard in coastal management and planning. However, recent research has highlighted that the static approach largely overestimates the flood extent compared to physics-based modeling, particularly in low-lying areas or in the presence of coastal defense structures (Sanders et al., 2024). Vousdoukas et al. (2016b) showed that "bathtub" methods can lead to an overestimation of the inundated areas of more than 200%. On the other hand, physic-based models specialized for coastal hydro- and morphodynamics, such as Delft3D (Deltares, 2024) and XBeach (Roelvink et al., 2009), represent optimal tools for the reproduction of complex processes leading to coastal inundation. However, they present the disadvantages of increased computational costs, making their application unfeasible to the large scales, and the requirement of detailed information about the nearshore topography. Other intermediate solutions exist, such as those taking into account just some aspects of the flooding hydrodynamics (Breilh et al., 2013; Dottori et al., 2018; Perini et al., 2016), or those defined as dynamic reduced complexity models, such as LISFLOOD-FP (Bates et al., 2010).

In this study, process-based modeling was used since the analysis was performed for small-scale domains for which the knowledge of the topography was quite detailed and refined. Specifically, wave propagation from the offshore to the nearshore was modeled through the wave-averaged Delft3D solver, while the nearshore wave evolution and inland penetration were reproduced using the XBeach model in the phase-resolving mode. Moreover, an evaluation of submerged breakwaters adaptation to CC was performed for one of the test sites, Pesaro (IT), that resulted to be highly impacted by coastal flooding.

Section 2 describes the five locations where the analysis was performed, the data collection and analysis to identify the forcing actions, and the model chain used to simulate future inundation scenarios. Results in terms of future drivers of coastal flooding, inundation maps, and adaptation of coastal structures are presented in Section 3, while Section 4 draws the Conclusions of the study.

2. Materials and methods

Assessment of the areas prone to flooding, mapping of the flooding extent and implementation of measures to reduce the risk of flooding are required by the European Floods Directive (2007/60/EC). The Directive aims at the assessment and management of flood risks to reduce the negative impacts of flooding on human health, economic activities, environment and cultural heritage in the EU, which are expected to increase in the near future due to CC. Following such Directive, we evaluated the inundation perimeters associated to high, medium and low probability of occurrence, using a model chain approach. The representative return periods (RP) for each probability of occurrence were RP = 20 years (high probability), RP = 100 years (medium probability) and RP = 200 years (low probability). To account for CC effects, the analysis was projected to 2070 under the IPCC very high emission scenario, referred to as RCP8.5 until the 5th Assessment Report, then substituted by the SSP5-8.5 in the 6th Assessment Report. This new definition of the scenario combines the very high level of radiative forcing in 2100 with the socio-economic assumption of a rapid growth of the global economy based on the exploitation of abundant fossil fuel resources (IPCC, 2023). An evaluation of the flood extent was already provided in the Marche Region ICZM Plan, but the cyclical nature of the Directive, which requires Member States to review and update flood risk maps every 6 years, suggests to re-assess the flood risk with an improved methodological approach. The procedure used in this study presents two main improvements with respect to the simple one adopted in the ICZM Plan. First, the numerical modeling of future inundation scenarios provides more realistic and detailed results than the ones obtained with a simple "bathtub" method, typically characterized by a large overestimation of the flooding extent. This is due to the fact that "bathtub" methods generally do not consider wave dissipation processes. Actually, in the ICZM Plan, wave dissipation was accounted for, albeit in a very simplified way. A GIS model named in_CoastFlood (Perini et al., 2012), developed by Servizio Geologico, Sismico e dei Suoli of the Emilia-Romagna Region (SGSS-RER), and accounting for wave dissipation through a damping factor depending on the distance from the shoreline, was used. However, this was not sufficient to effectively reproduce the effects of real dissipation processes. Secondly, the effect of CC is considered in a more accurate manner, using projections of future forcing actions rather than just increasing of a given percentage the computed water levels, as it was done in the ICZM Plan. The suitability of such approach was already tested in Baldoni et al. (2024), whose results served as a scientific basis for the Marche Region to define specific adaptation strategies to put in place. A further improvement was done here in the definition of the forcings, as explained in Section 2.2.

The analysis was performed for five coastal locations along the Mid Adriatic Sea, as described in Section 2.1.

2.1. Test sites

Test sites were selected by the Marche Region considering the presence of coastal defense structures, harbor facilities and different sediment sizes (Table 1). The choice fell on locations that are highly vulnerable, both because of their strategic value (economic and touristic) and because of the presence of urban settlements that either historically were affected or nowadays are frequently subjected to coastal flooding.

Three sites (T1, T2 and T3) are located to the North of Ancona, while two (T4 and T5) are in the southern part of the region (Fig. 1).

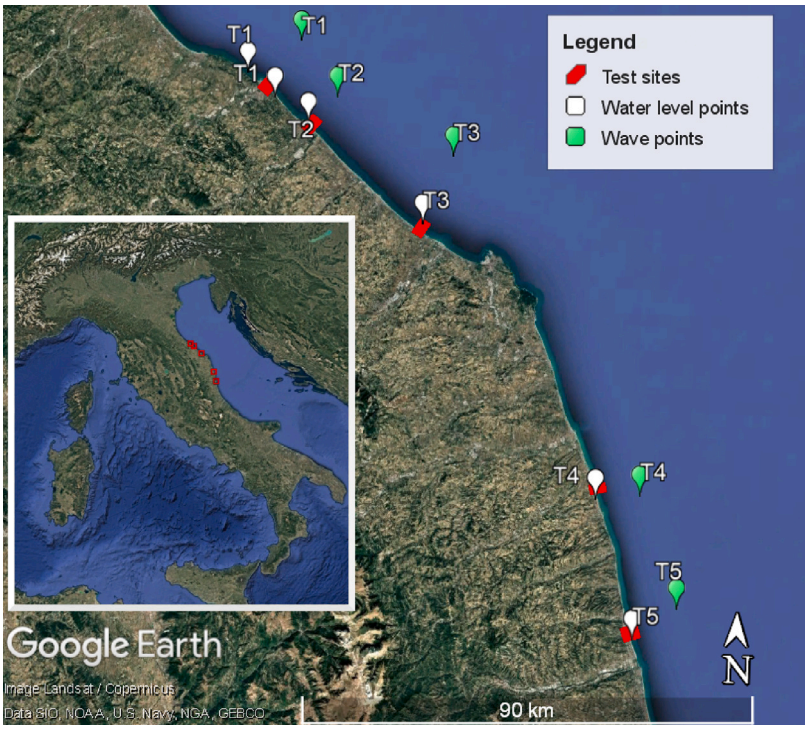

Fig. 1. Location of the test sites (red rectangles) along the Adriatic coast. A global view of Italy is given in the box on the left, while the rest of the figure provides a zoom on the interested coastline. White and green markers identify Copernicus grid points used for water level and wave data, respectively. (For interpretation of the references to color in this figure legend, the reader is referred to the web version of this article.)

Table 1
Characteristics of the five test sites analyzed: name, ID, type of coastal defense structures, type of sediment and length of the coastal stretch considered.

Site name	Site ID	Structure type	Sediment type	Length [km]
Pesaro	T1	Submerged and emerged breakwaters	Sand	2.66
Fano	T2	Free; submerged and emerged breakwaters	Gravel	2.50
Montemarciano	T3	Free; groynes	Gravel	2.40
Fermo	T4	Emerged breakwaters	Sand	1.76
San Benedetto del Tronto	T5	Harbor; emerged breakwaters; free	Sand	2.75

The Marche Region provided us with a high resolution (0.5 m × 0.5 m) topographic Lidar of the coastal zone plus some topo-bathymetric transects (2 or 3 for each site). Such detailed information was complemented with the online-available EMODnet bathymetry[1] dataset and regional digital terrain model,[2] characterized by a resolution of 100 m and 20 m, respectively.

2.2. Data collection and analysis

To simulate future coastal flooding, we considered different forcings, namely sea level rise, tide, storm surge and waves. Their collection and analysis is described in the following sections.

2.2.1. Sea level rise

The sea level rise for the year 2070 under the SSP5-8.5 scenario was provided by the Sea Level Projection Tool[3] of the NASA Sea Level Change Portal, a tool to visualize and download the sea level projection data from the IPCC 6th Assessment Report (IPCC, 2023). Considering the location of the considered sites, the same value of sea level rise was obtained, equal to 0.36 m.

2.2.2. Tide and storm surge

Tidal and storm surge forcings came from projections of water level data. Such projections were retrieved from the datasets of the Copernicus Climate Change Service (C3S) consisting in a timeseries with 10 m temporal resolution and spatial resolution of 0.1° (ECMWF, 2024). Water level dataset includes an historical reanalysis based on ERA5 data, covering the period 1976–2017, and two Representative Concentration Pathway (RCP) scenarios, RCP4.5 and RCP8.5, covering the periods 2070–2100 and 2040–2070, respectively. The astronomical tide is a deterministic variable that can be calculated based on the relative positions of celestial bodies, while storm surge is a stochastic variable influenced by meteorological factors, making it more suitable for long-term analysis. Although a considerable amount of literature addresses non-linear interactions between tides and surge, particularly through the well-known concept of skew surge (e.g., Ragno et al., 2023), this approach may not be appropriate for the specific case study at hand. Skew surge was initially studied in macrotidal sites, where the phase lag induced by tide-surge interactions leads to significant apparent residuals and thus their strong overestimation. This effect is less relevant in micro-tidal environments like those considered in this study. Moreover, if the skew surge approach is adopted, there is a risk of underestimating surge levels when extreme sea levels occur during low tide phases. Therefore, to mitigate the risk of any potential underestimation that could pose significant challenges for

[1] EMODnet Digital Bathymetry (DTM 2022). EMODnet Bathymetry Consortium. https://doi.org/10.12770/ff3aff8a-cff1-44a3-a2c8-1910bf109f85.

[2] DTM Marche Region. https://www.regione.marche.it/Regione-Utile/Ambiente/Cartografia-e-informazioni-territoriali/Repertorio#DTM.

[3] https://sealevel.nasa.gov/ipcc-ar6-sea-level-projection-tool.

effective coastal area management, the present analysis utilized the storm surge values obtained from the Global Tide and Surge Model v3.0 (GTSMv3.0) which is a depth-averaged hydrodynamic model with global coverage that dynamically simulates tides and storm surges. The use of the unstructured Delft3D-FM (Kernkamp et al., 2011) allows for a smart distribution of resolution, which leads to high accuracy at relatively low computational costs. The meteorological forcing derives from the HIRHAM5 regional climate model (Christensen et al., 2007) of the Danish Meteorological Institute (DMI), member of the Euro-CORDEX ensemble, while relative sea level rise fields corresponding to the two emission scenarios considered are taken from the ensemble-mean of the Coupled Model Intercomparison Project Phase 5 (CMIP5). For more details, the reader is referred to ECMWF (2024). Data were downloaded, for the RCP8.5 scenario, from the grid points nearest to the test sites, as indicated by white markers in Fig. 1. For Pesaro (T1), the mean between two points at the borders of the domain of interest was performed.

Given the micro-tidal nature of the site, to give conservative results, the tidal forcing was chosen as the maximum astronomical tide of the thirty-year period considered (2040–2070).

For the storm surge, an extreme value analysis was performed with different return periods (RP20, RP100 and RP200). A Peak Over Threshold (POT) procedure allowed us to identify significant independent events as those exceeding the threshold 0.4 m and separated by at least 12 h (data declustering). Such threshold was chosen large enough to focus the analysis on extreme events and small enough to ensure a representative number of events. A mono-variate analysis was then carried out to find the probabilistic distribution that best fitted with the data among Three-Parameter Weibull, Log-Normal, GEV and Gamma. The Maximum Likelihood Estimation (MLE) was used to obtain the distribution parameters. First, for each fitted distribution, the Anderson–Darling test was performed to verify the failure to reject the null hypothesis at the 5% significance level. If the test fails to reject the null hypothesis, different statistical parameters are computed such as the Root Mean Square Error ($RMSE$), the coefficient of determination (r^2), the p-value and the Anderson–Darling test statistic (A^2) defined as follows:

$$RMSE = \sqrt{\frac{\sum_{i=1}^{M}(y_o - y_d)^2}{M}} \tag{1}$$

$$r^2 = 1 - \frac{\sum_{i=1}^{M}(y_o - y_d)^2}{\sum_{i=1}^{M}(y_o - \overline{y_o})^2} \tag{2}$$

$$A^2 = -M - \sum_{i=1}^{M}[\ln(F(y_{o,i})) + \ln(1 - F(y_{o,M+1-i}))] \tag{3}$$

where y_o are the observed values with mean value $\overline{y_o}$, y_d are the distribution values and M is the number of samples. $F(y_{o,i})$ represents the cumulative fitted distribution in correspondence of the ith observed value. The p-value is computed analytically based on A^2 (D'Agostino, 1986). The best distribution was selected as the one yielding the minimum values of $RMSE$ and A^2, and the maximum values of r^2 and the p-value, to minimize the differences between predicted and actual data points, with special focus on the tail of the distribution. The main statistical parameters of storm surge distribution for the five test sites are summarized in Table 2. From these results, Weibull and Gamma distributions are those that better represent observed data. The $RMSE$ values are in the range 0.9–1.5 cm. p-values are always larger than 0.05, meaning that there are not significant differences between the observed and modeled distributions.

Table 2
Main statistics of storm surge distributions for the five test sites analyzed.

Site name	Site ID	Distribution	RMSE	r^2	p-value	A^2
Pesaro	T1	Gamma	0.012	0.990	0.981	0.226
Fano	T2	Weibull	0.009	0.994	0.833	0.415
Montemarciano	T3	Weibull	0.014	0.985	0.615	0.635
Fermo	T4	Gamma	0.011	0.987	0.973	0.246
San Benedetto del Tronto	T5	Weibull	0.015	0.971	0.619	0.631

2.2.3. Waves

The future wave climate for each site was assessed using projected timeseries of hourly wave data (Caires and Yan, 2020) from the C3S. Data are obtained with a standalone version of the Wave Model (WAM), referred to as Stand Alone WAM (SAW), of the European Center of Medium-Range Weather Forecast (ECMWF). The validation of SAW wave hindcast data against observations is documented in ECMWF (2024). The wind forcing employed to simulate the wave climate comes from the regional climate model HIRHAM5. The dataset includes an historical reanalysis and two RCP scenarios, RCP4.5 and RCP8.5. For the present work, only the RCP8.5 scenario was used. Data are provided for the European coastline along the 20 m bathymetric contour, with a horizontal resolution of ~30 km. For each site, the nearest grid point was chosen, indicated with green markers in Fig. 1, and wave roses were produced (Fig. 2). This analysis allowed us to identify the main sectors for which to perform the extreme value analysis. A bivariate extreme value analysis of significant wave height and peak wave period is crucial for accurately assessing the joint probability of wave climate parameters, which directly influences coastal engineering design and risk assessments, such as flooding and erosion, under extreme conditions (Coles, 2001; Montes-Iturrizaga and Heredia-Zavoni, 2015). Such approaches provide more robust insights compared to univariate methods, especially in understanding the correlation between wave energy and storm dynamics in environments like the Adriatic Sea (Ragno et al., 2023). This analysis is aimed at computing an extreme pair of wave height-peak period ($H_s - T_p$). Although some sites present a bimodal wave climate, the analysis was performed only for the sector that presents the most frequent and highest waves: 45° ± 7.5° for T1, 60° ± 7.5° for T2 and T3, and 105° ± 7.5° for T4 and T5. Following the procedure applied for the storm surge analysis, a declustering step was first performed, using as threshold the value of H_s associated to the 90th percentile and considering a minimum time span between two following peaks of 12 h. On such dataset of H_s and T_p pairs, the two marginal distributions were identified among Three-Parameter Weibull, Log-Normal, GEV and Gamma using MLE criterion for the choice of the parameters and the $RMSE$, r^2, p-value and A^2 criterions for the choice of the best distribution. The joint distribution between these parameters was modeled using a copula approach, which allows for the exploration of the dependence between wave height and peak period. Several types of copulas were tested, including both Archimedean (Gumbel, Clayton and Frank) and elliptical copulas (Student's t) and their parameters were estimated using the MATVines tool (Coblenz, 2021) that applies the Akaike Information Criterion (AIC) for model selection. The graphical representation of the copula results is usually done by means of the so-called "environmental contours", which are curves in the $H_s - T_p$ plane associated to different return periods, obtained with the Inverse First-Order Reliability Method (IFORM) (Winterstein et al., 1993). These contours are essential tools for coastal engineering applications, providing insights into the joint occurrence of extreme environmental conditions at specific return periods (Eckert-Gallup et al., 2016; Saranyasoontorn and Manuel, 2004; Huang and Dong, 2021). Each of the point constituting an environmental contour is associated to a specific return period. However, for most of coastal applications, pinpointing a specific pair of variables associated to a specific return period is fundamental to plan further analysis. Different criteria can be applied depending on the type of application for which the contours are computed (Mikulić and Parunov, 2023; Clarindo and Guedes Soares, 2024; Ross et al., 2020). The goal of this study is to characterize coastal flooding. Both wavelength and wave height play a significant role in this phenomenon. The wave energy flux is widely recognized as one of the main drivers of coastal morphodynamics. Extreme waves transfer

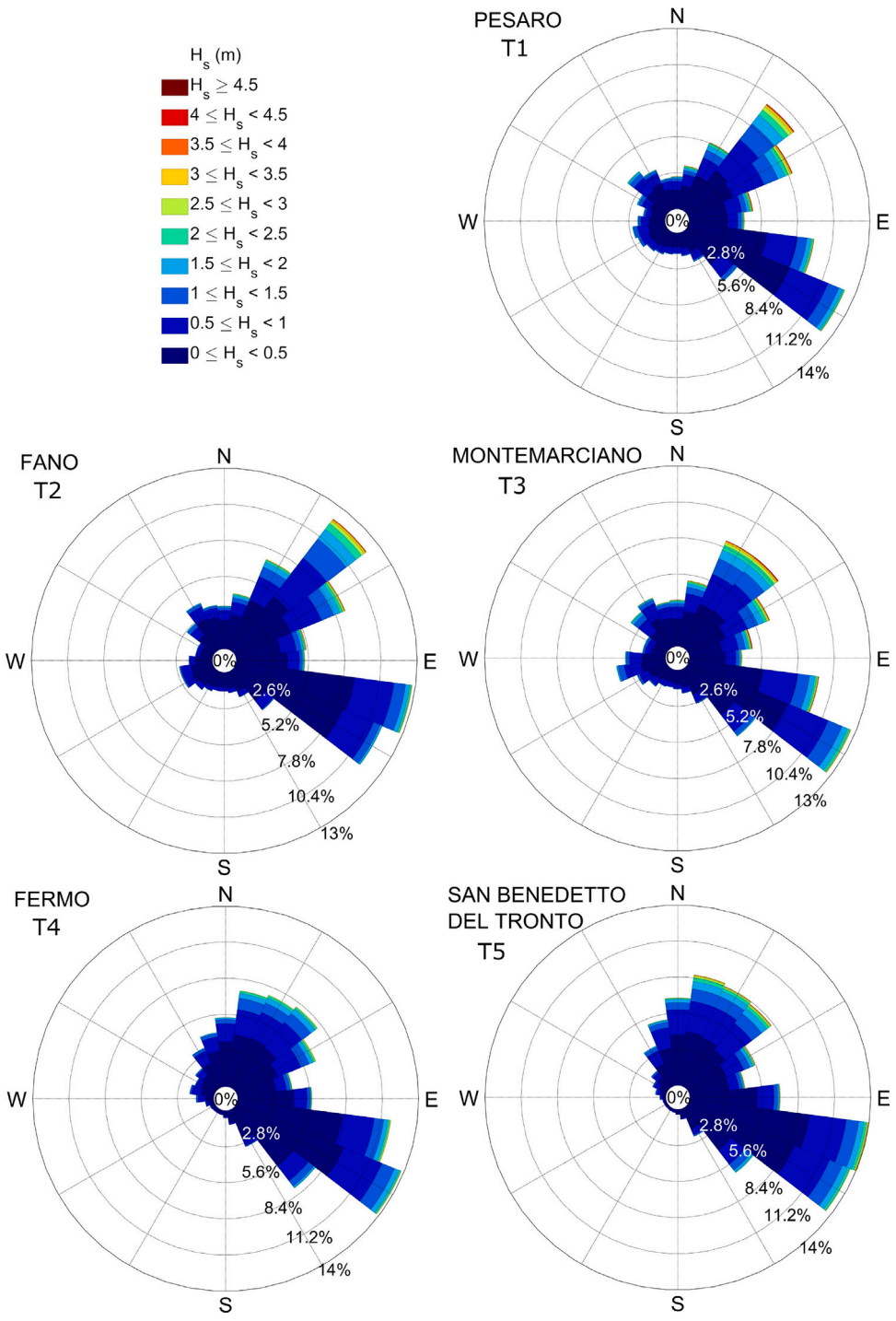

Fig. 2. Wave roses for the five test sites. (For interpretation of the references to color in this figure legend, the reader is referred to the web version of this article.)

large amounts of energy to the coast, driving inundation processes, among others (Vousdoukas et al., 2016b; Bertin et al., 2012). Wave energy flux is, therefore, a crucial parameter for assessing coastal hazard risk associated with extreme water levels (Mentaschi et al., 2017). The pairs $H_s - T_p$ to force the numerical simulations are hence identified based on the maximum energy flux (P) computed as:

$$P = \frac{1}{8}\rho g H_s^2 C_g \tag{4}$$

where ρ is the water density, g is gravity and $C_g = 0.5C$ is the wave group celerity, computed as half the phase velocity.

A more detailed description of the applied method for the application of copulas and for the computation of environmental contours can be found in Corvaro et al. (2025).

2.3. Model chain approach

The model chain approach used to simulate future coastal flooding conditions relies on environmental forcings derived from climate projections. Specifically, the wave and storm surge values associated with different return periods were obtained from an analysis of the Copernicus Climate Change Service (C3S) dataset. While this study relies on

climate projections from a single source to ensure consistency across environmental forcings, we acknowledge that incorporating multiple climate models would provide a more comprehensive assessment of uncertainty. Future research should explore additional projections from different climate models to quantify the range of possible outcomes and further refine the robustness of coastal impact assessments. The model chain approach used to simulate future coastal flooding conditions consists of two solvers, Delft3D (https://oss.deltares.nl/web/delft3d) and XBeach (https://oss.deltares.nl/nl/web/xbeach). Delft3D is a wave-averaged model that gives a wave description averaged over the wave period. Such model allows one to simulate the wave propagation over large domains in relatively short time. However, it has limitations when dealing with large seabed gradients, as, for example, near harbors or coastal defense structures. For this reason, the wave-resolving model XBeach, which computes velocities and water levels within the wave period, was also used. Delft3D was used to transfer the wave from a depth of 20 m, which is where the wave data were provided by C3S, to a depth of 8–9 m. The resulting wave characteristics were used to force the XBeach detailed model that computed the wave propagation towards the shoreline and provided the inundation perimeters. Such model chain approach has been used to simulate coastal flooding in various contexts, from that caused by present forcing conditions on relatively steep beaches (Postacchini et al., 2019), to that induced by future meteocean actions on mildly sloping coastlines (Baldoni et al., 2024).

2.3.1. Wave propagation from 20 m depth to the nearshore

Delft3D is a modeling suite, developed by Deltares, widely used and validated for coastal locations all over the world, which allows one to simulate hydrodynamics, sediment transport and morphological evolution, wave generation and propagation, water quality, and bio-ecological processes in rivers, estuaries and coastal environments. It consists of several independent modules that can interact one with each other. For this study, the WAVE module (Deltares, 2024) was used to propagate a JONSWAP-type wave spectrum towards shore. In Delft3D, the third-generation model SWAN (Booij et al., 1999), developed at the Delft University of Technology, is used as wave-driver. The SWAN model is based on the discrete spectral action balance equation and has been successfully validated and verified in several laboratory and field cases (Ris et al., 1999).

The wave forcing to be applied at the offshore boundary is given at 20 m water depth (see Section 2.1 and Table 4), which is reached around 13 km offshore from the Marche coastline. Therefore, a 100 m × 100 m structured grid, extended up to 20 m water depths and aligned with the coastline, was built for each test site (blue grid in Fig. 3a). Parallel to the coastline, the grids were extended enough to avoid "boundary effects" possibly affecting the dynamics in the areas of interest. A more detailed grid, with 10 m resolution and extended up to some hundred meters inland, was created to properly model the inundation (red grid in Fig. 3a). Such grid fitted the land-water boundary better and was used also for the XBeach computations, refined up to 5 m × 5 m. Grids were connected through a nesting procedure, implemented in the WAVE module to transfer the information between different domains. Bathymetries were created by combining the available datasets, described in Section 2.1, prioritizing those with higher resolution (Fig. 3b). Coastal defense structures were modeled directly changing the terrain elevation as shown in Table 3. The roughness coefficient was varied to account for different sediment types and urban areas, setting it to 0.020 $s/m^{1/3}$, 0.035 $s/m^{1/3}$ and 0.070 $s/m^{1/3}$, respectively for sandy beaches, gravel beaches and urbanized areas.

The offshore boundary condition consisted of waves generated by a time series of JONSWAP spectra characterized by significant wave height, peak period, and direction. The time series lasted 8 h, starting with $H_s = 1$ m and reaching the peak value, as indicated in Table 4, at the sixth hour. Then, waves decreased symmetrically to the increasing branch. The wave period and direction were kept constant throughout the entire time series to ensure that the maximum wave steepness was reached at the peak of the simulated storm, coinciding with the occurrence of maximum flooding. This choice was made because the inundation extent is primarily controlled by the storm peak rather than by the full variability of wave dynamics. Therefore, keeping the wave period constant does not significantly affect the estimation of maximum flooding, which remains the focus of this study.

Table 3
Elevation assigned to different type of coastal defense structures.

Structure type	Elevation [m a.s.l.]
Emerged breakwaters	+1.5
Submerged breakwaters	−0.7
Emerged groynes	+1.5
Submerged groynes	−0.7
Adherent breakwaters	+1.5

2.3.2. Wave propagation from the nearshore to shore

To propagate waves up to shore and compute the inundation extent, the open-source XBeach model was used (Roelvink et al., 2009). It allows to simulate short waves transformation processes, such as refraction, shoaling and breaking, phenomena related to long waves (infragravity waves), set-up, run-up, overwash and flooding. XBeach has three working modes, namely stationary, surfbeat (non-stationary) and wave-resolving (non-hydrostatic). Here, the third mode was used, whose main advantages are the inclusion of the incident-band (short wave) runup and overwashing, the direct resolution of wave asymmetry and skewness, and the computation of wave diffraction, non negligible around breakwaters and harbor facilities. The inclusion of all these processes requires longer computational times. The non-hydrostatic module is based upon (Stelling and Zijlema, 2003) and solves the non linear shallow water equations, including a non-hydrostatic pressure term. The model has been validated in both experimental and field applications (Den Bieman et al., 2024; Smit et al., 2010; Amini and Marsooli, 2023).

The wave characteristics computed by Delft3D WAVE were extracted at the center of the offshore boundary of the inner grid and used to force the XBeach model. Also for XBeach, the imposed forcing was a timeseries of 2D JONSWAP spectra, whose characteristics are summarized in Table 5. Furthermore, the contribution of the SLR, storm surge, meteorological tide, wave set-up and run-up were also accounted for. Wave set-up and run-up were computed by the model. A sinusoidal tidal timeseries was built and added to an initial water level equal to the sum of SLR and storm surge. The peak of the tidal timeseries, corresponding to the highest astronomical tide provided by the C3S dataset, was made simultaneous with the storm peak to consider the most pessimistic scenario. Water level forcings are reported in Table 4.

2.3.3. Adaptation of coastal defense structures

For one test site, namely Pesaro (T1), and only for the 100-year return period scenario, we tested a modified breakwater elevation as an adaptation measure to climate change. This example was chosen as representative of similar behaviors observed along the Marche coast, focusing on the general response of submerged breakwaters. A comprehensive analysis of adaptation strategies for beach defense structures, considering multiple return periods and geometry variations, is beyond the scope of this study. Adaptation of emerged breakwaters was achieved by increasing of 1 m their elevation, considering the sum of future SLR and storm surge, i.e. 1.67 m (Table 4), and the typical dimension of the boulders employed to build breakwaters. For submerged structures, Marini et al. (2020) evaluated which is the best adaptation strategy between the enlargement of the berm width and the increase of the structure height, keeping the same volumes involved and, subsequently, almost the same costs. The authors found that below a certain threshold for the sea elevation, equal to 0.5 m, the

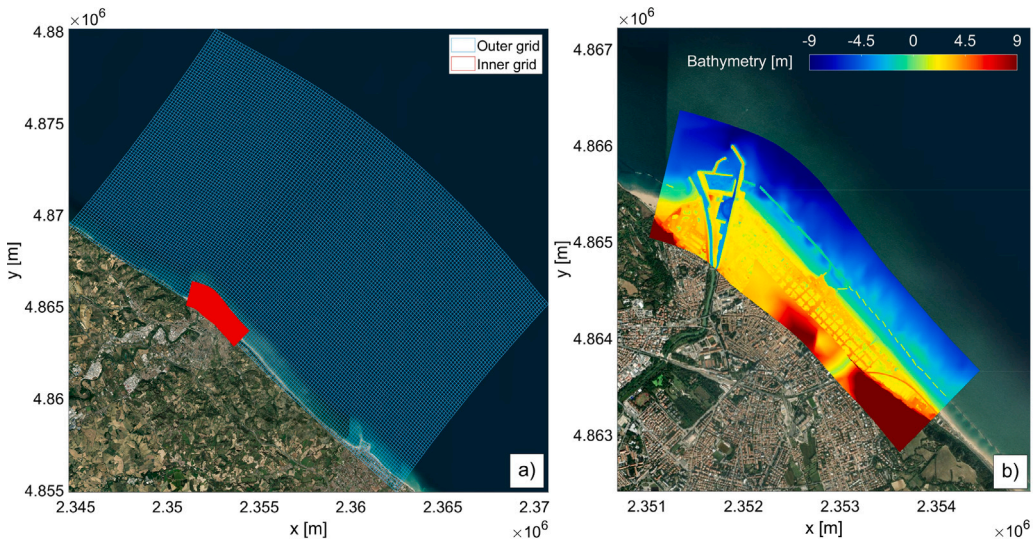

Fig. 3. Grids (a) and bathymetry for the inner grid (b) for Pesaro (T1). (For interpretation of the references to color in this figure legend, the reader is referred to the web version of this article.)

enlargement of the berm width is more effective than the increase of the breakwater elevation, and vice-versa. Further, when the sea level variation is very small, their results showed that elevating the structure is even worse than no adaptation at all. However, since in our test case the sea elevation is greater than 0.5 m, we decided to increase the elevation of the submerged breakwaters. To evaluate the optimal freeboard R_c that minimizes the cross shore beach profile recession ΔY, the semi-analytical model by Marini et al. (2022) was applied. To feed the model, we used site-specific characteristics (a beach slope of 1/35, a berm width of 19 m and a water depth of 3 m) and projected forcings reported in Table 4 (a sea elevation of 1.67 m, an offshore wave height H_0 of 6 m and a period of 10 s). Fig. 4 shows that the optimal value of R_c is 0.5 m above the present sea level, which means an increase of the structure height of 1.2 m. If one refers to the simulated future scenario, such configuration corresponds to a submergence of 1.17 m. Fig. 4 also highlights that a further freeboard increase leads to a larger beach profile recession until the structure becomes emerged, condition that allows to reduce the wave height and the consequent shoreline recession. This occurs because the submerged breakwaters are built to generate breaking when waves pass over them, with a consequent energy dissipation and reduction of the transmitted wave height. However, this mechanism also causes a rise in the level (piling-up) behind the structures, which increases at the increase of the freeboard. Therefore, if the submergence of the breakwaters decreases, the negative effect of the piling-up overcomes the positive effect of the wave height reduction, leading to larger shoreline recessions.

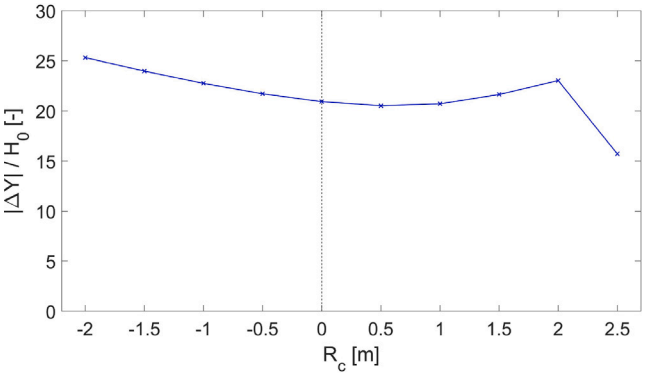

Fig. 4. Results of the semi-analytical model by Marini et al. (2022), showing the non-dimensional beach profile recession $|\Delta Y|/H_0$ depending on the breakwater freeboard R_c.

3. Results and discussion

The results of the extreme value analyses performed to obtain the future forcings for the simulations are summarized in Section 3.1. Sections 3.2 and 3.3 present the numerical results in terms of inundation perimeters and levels, while findings regarding adaptation of coastal defense structures are outlined in Section 3.4.

3.1. Future forcings

Results of the monovariate and bivariate analyses for the storm surge and waves are, respectively, shown in Figs. 5 and 6 and summarized in Table 4.

The SLR in front of the Marche coastline is projected to be 0.36 m in 2070 under the SSP5-8.5 scenario. The astronomical tide and storm surge increase moving from the South to the North of the coastline (from T5 to T1), reflecting the overall behavior of the Adriatic Sea (Medvedev et al., 2020; Schwab and Rao, 1983; Pasquali et al., 2015; Vousdoukas et al., 2016a).

Results of wave propagation towards the shore are illustrated in both Table 5 and Fig. 7. The former reports the parameters of the wave spectra computed by SWAN at a water depth of around 8–10 m. The comparison with the same values at 20 m, shown in Table 4, highlights the reduction of both wave height and period as the wave approaches the coast and the refraction of wave fronts, which tend to align parallel to the shoreline. Similar findings are displayed by Fig. 7a and b, showing the wave propagation from the outer to the inner grid of the Delft3D domain for Pesaro (T1). Moreover, the difference in the modeling of wave propagation between phase-averaged and phase-resolving model is clearly visible comparing Fig. 7b and c. While in Delft3D the wave is averaged over the period, XBeach solves the wave phase, this resulting in the visualization of the sea state variable H_s in the former case, and of single waves in the latter. Better results of XBeach with respect of Delft3D in terms of wave interaction with structures are also evident. Delft3D reproduces the wave height reduction behind breakwaters, but diffraction processes are not properly simulated. On the other hand,

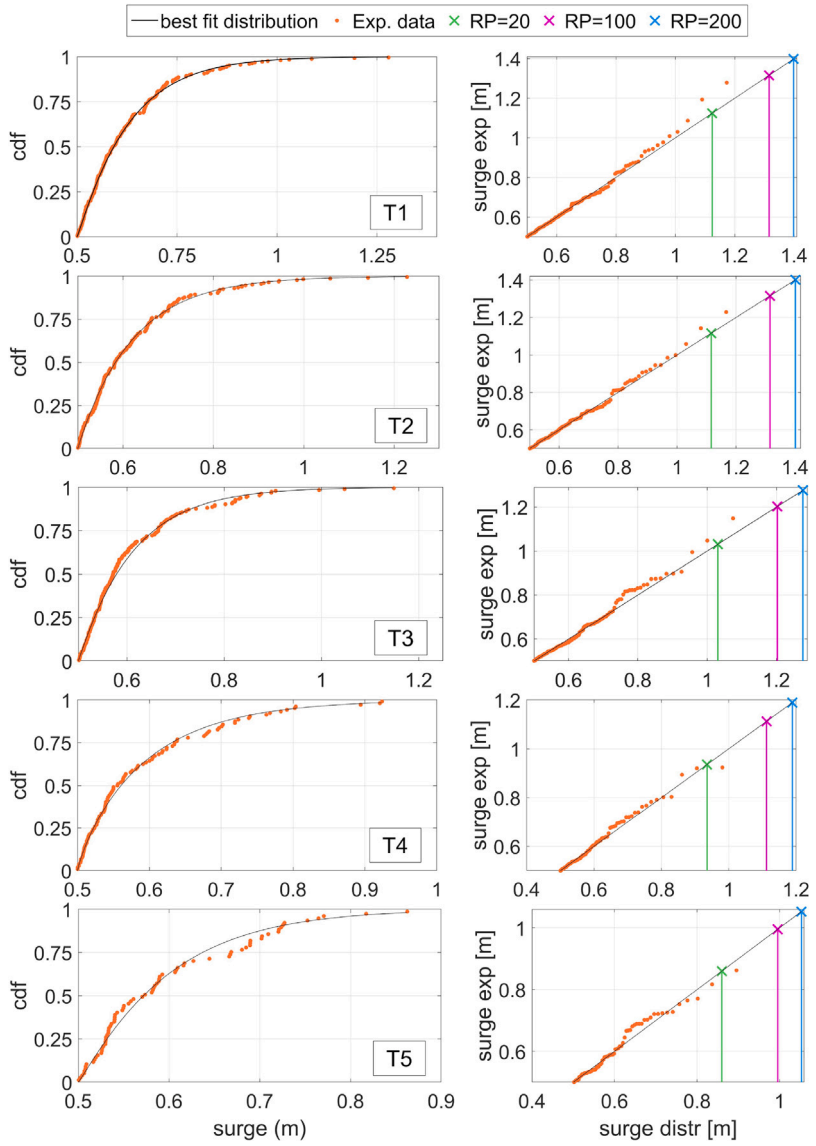

Fig. 5. Results of the extreme value analysis for the storm surge. Panels to the left and right show the best cumulative distribution function (cdf) and the values associated to different return periods, respectively. Orange dots represent the experimental data (from the C3S dataset); the black line identifies the best distribution; green, magenta and blue crosses represent, respectively, the storm surge with 20, 100 and 200-years return periods. (For interpretation of the references to color in this figure legend, the reader is referred to the web version of this article.)

Table 4
Water levels and wave forcing (storm surge, astronomical tide, SLR, H_s, T_p and direction) for 20, 100 and 200-years return periods. Wave parameters are those at the peak of the simulated storm.

	Water levels [m]					Waves [m, s, °N]						
	Storm surge			Tide	SLR	H_s			T_p			Dir
RP	20	100	200	All	All	20	100	200	20	100	200	All
T1	1.12	1.31	1.40	0.48		5.07	5.94	6.29	9.71	10.51	10.88	45
T2	1.11	1.31	1.40	0.45		4.61	5.84	6.36	9.74	10.82	11.30	60
T3	1.03	1.20	1.28	0.37	0.36	4.87	6.10	6.63	8.76	8.90	8.92	60
T4	0.93	1.11	1.19	0.33		4.21	5.23	5.67	10.79	11.82	12.24	105
T5	0.86	0.99	1.05	0.35		4.90	6.07	6.58	10.78	11.63	11.92	105

XBeach well models the diffraction of waves over emerged breakwaters and harbor jetties.

3.2. Coastal flooding at different test sites

Inundation maps at the peak of the simulated wave storm are shown in Fig. 8 for a 100-year return period scenario. The maps show water depths in the flooded areas, highlighting the different response of the test sites. In terms of inundation extent, the most impacted site is T5 with 0.54 km^2, followed by T2 with 0.49 km^2, T1 with 0.48 km^2, T4 with 0.42 km^2 and T3 with 0.17 km^2.

In the ICZM Plan, the entire coast of the Marche Region (subdivided in several transects) is analyzed in terms of accretion/retreat by computing an index. Such index I is the ratio between the mean

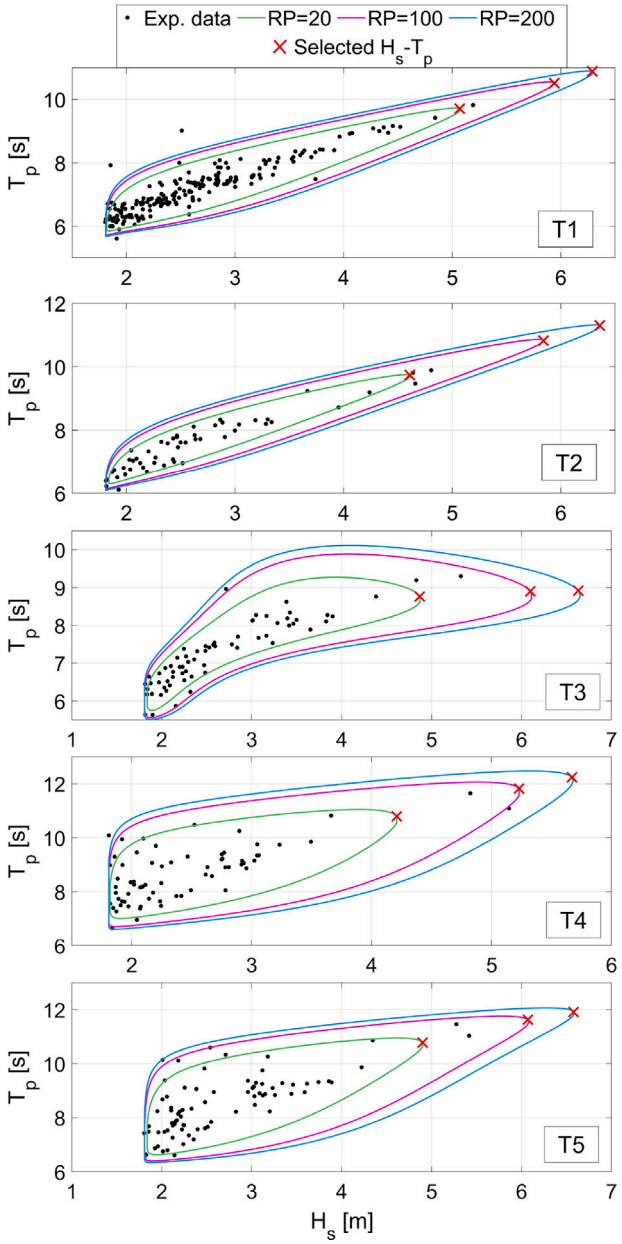

Fig. 6. Environmental contours for the test sites: black dots give the experimental data (from the C3S dataset); green, magenta and blue curves represent the contours for RP20, RP100 and RP200, respectively; red crosses highlight the couple H_s-T_p selected to force the simulations with. (For interpretation of the references to color in this figure legend, the reader is referred to the web version of this article.)

Table 5
Characteristics of the wave spectra computed by SWAN and used as offshore boundary conditions for XBeach. The values are those at the peak of the simulated storm.

	H_s [m]	T_p [s]	Dir [°N]	H_s [m]	T_p [s]	Dir [°N]	H_s [m]	T_p [s]	Dir [°N]
RP	20			100			200		
T1	3.88	9.05	41.62	4.08	9.93	41.17	4.15	10.27	40.90
T2	3.50	8.99	49.61	3.94	10.16	49.49	4.03	10.61	49.32
T3	3.63	8.00	48.02	3.98	8.29	47.70	4.04	8.38	47.63
T4	3.03	9.96	88.33	3.77	10.96	88.19	4.04	11.36	88.16
T5	3.87	9.96	92.30	4.41	10.82	92.30	4.52	11.19	92.25

accretion/loss of beach in some reference periods and the beach area bounded by the "reference shoreline" (Regione Marche, 2019). Results are divided into four classes depending on the value of I: retreat ($I \leq -10$), tending to retreat ($-10 \leq I \leq 0$), tending to accretion ($0 \leq I \leq 10$), accretion ($I \geq 10$).

T1 is located in the northern part of the Marche coastline and is identified as an area tending to accretion or retreat, depending on the transects. Some video/press reports on some severe coastal flooding occurred in 2015, showing that water levels reached 3.2 m a.s.l., thus interesting some urban areas (where the oblique emerged breakwater is located). XBeach results highlight the high inundation hazard for the area located South of the harbor, where the flooding extends for about 400 m inland, affecting a large portion of the urban area.

T2 is also located in the North of Marche and presents a worse situation with respect to T1. The majority of the area is classified as tending to retreat/in retreat and some interventions have already been put in place or planned in the ICZM Plan. As for T1, some evidence of past floods showed that water levels exceeded 3.2 m a.s.l., causing damages to the urban area North of the groyne. The map in Fig. 8 shows a maximum water penetration of around 190 m inland, affecting roads, houses and commercial buildings.

T3 has the largest beach slope (around 90% for the emerged profile) and, therefore, is characterized the lowest inundation extent. However, such site is also characterized by the presence of a coastal road adjacent to the beach at about 2.2 m a.s.l., at a maximum distance from the sea of around 35 m, that gets frequently flooded (on average, twice a year (Regione Marche, 2019)). Behind such street, there are houses and the railway, also affected by the inundation. Thus, even a small inundation (maximum 90 m inland) is enough to cause damages to infrastructures and buildings. The Marche Region has already identified T3 as an area subjected to erosion and with high priority of intervention: both maintenance and new interventions were programmed in the ICZM Plan, including beach nourishment and emerged breakwaters.

T4 and T5 are located in the southern part of the Marche Region, the former identified as tending to accretion, the latter as tending to accretion/in accretion. The simulated inundation extends up to 200 m and 130 m inland, respectively for T4 and T5, without considering the harbor area. The port facility in San Benedetto del Tronto (T5) is largely flooded, as also the adjacent recreational area and buildings (see last panel of Fig. 8). For T4, the inundation interests some buildings and small portions of streets.

Despite the presence of coastal defense structures, the simulated storm causes the complete flooding of beaches and summer facilities in all the test sites, highlighting the need to adapt the structures to CC.

3.3. Effect of different return periods

To observe the effect of different return periods, we selected the site of Pesaro (T1), which is highly exposed to coastal flood risk, particularly in the urban area located South of the harbor. Fig. 9 shows the inundation maps for 20, 100 and 200-years return periods. The flood extent increases from 0.36 km^2, to 0.48 km^2, to 0.57 km^2, the water penetrating up to around 300 m, 400 m and 500 m inland. Also water depths become higher at the increase of the return period. Results for the other four test sites are reported in the Supplementary Material (Figures s1, s2, s3, s4).

Fig. 10 shows the comparison between the inundation perimeters computed by XBeach and those calculated in the ICZM Plan (Regione Marche, 2019). In the Plan, perimeters were determined using a "bathtub" approach, which means performing an intersection between the horizontal plan corresponding to the sea elevation and the regional DTM. The sea elevation was evaluated for 20 and 100-years return periods as the sum of several contributions, namely storm surge, astronomical tide and set-up, and wave run-up computed with the empirical formulation by Stockdon et al. (2006). The obtained values were then increased by 10% to account for CC, resulting in 1.79 m

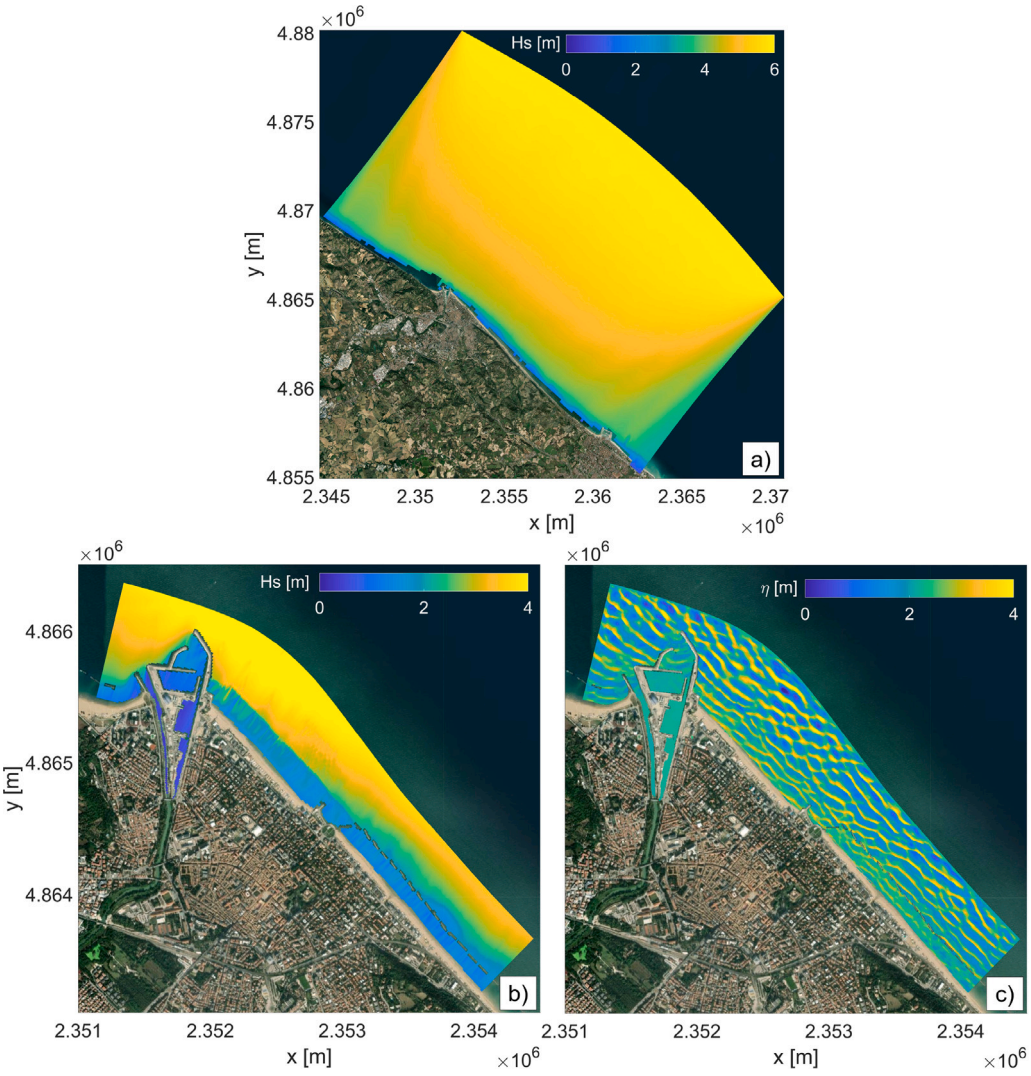

Fig. 7. Wave propagation at the peak of the storm for Pesaro (T1): (a) significant wave height in the Delft3D outer grid; (b) significant wave height in the Delft3D inner grid; (c) sea surface elevation (η) in XBeach. Maps are limited to the land-water boundary at the beginning of the simulation (no flooding is shown here). (For interpretation of the references to color in this figure legend, the reader is referred to the web version of this article.)

(RP20) and 2.45 m (RP100). For the low probability of occurrence, the Plan defined the flooding perimeter through an observation dataset of extreme events (RP > 100). This is likely the reason why the XBeach perimeters associated to the 200-years return period are less extended than those estimated in the Plan, as shown in the last panel of Fig. 10 and in the Supplementary Material, where results for the other four test sites are shown (Figures s5, s6, s7, s8). The modeled inundation is larger than that computed in the Plan for the high probability of occurrence (RP20, top panel of Fig. 10), while the two perimeters alternate for the 100-years return period scenario, the red one (XBeach) being either less or more extended than the green one (ICZM Plan), respectively near the port and to the South. Differences are mainly related to the different methods of computation. The "bathtub" approach, even if relatively simple and easy to apply to large domains (e.g. to evaluate the areas more prone to inundation for an entire region), does not account for wave dissipation processes, this typically resulting in an overestimation of flooded areas. On the other hand, numerical simulations model the wave propagation in more detail and provide more realistic results. However, to be effective, such procedure requires a thorough knowledge of the site characteristics, including high resolution bathymetry, topography, type of structures and forcing actions. In addition, computational power is also essential to produce results in reasonable times. Other differences between the flooded areas can be attributable to manual modifications that were made in the perimeters of the ICZM Plan based on direct observations.

3.4. Adaptation of coastal defense structures

To evaluate the adaptation of breakwaters to CC, a simulation was run for Pesaro (T1) under the 100-years return period scenario, changing the elevation of both emerged and submerged breakwaters, as explained in Section 2.3.3. Results showed that the inundation perimeters varied just slightly, with the flooding extent becoming larger behind submerged breakwaters, while reducing behind emerged structures (see Figure s9 in the Supplementary Material). To better understand the effect of the adaptation, results are compared in terms of water levels, as shown in Fig. 11a. Water depths in the area protected by submerged structures increase in the case of adapted breakwaters, while the opposite occurs for emerged breakwaters. The worsening of the flooding extension and levels is caused by the piling-up occurring behind submerged breakwaters. In fact, even if the wave height reduces after breaking above the structures (Fig. 11b), also an increase of water levels behind the breakwaters occurs (Fig. 11c, red ellipse), leading to a greater inundation extent and higher water depths in the flooded areas. The set-up induced by low-crested structures within the protected zone is due to wave overtopping and increases until a level is reached that

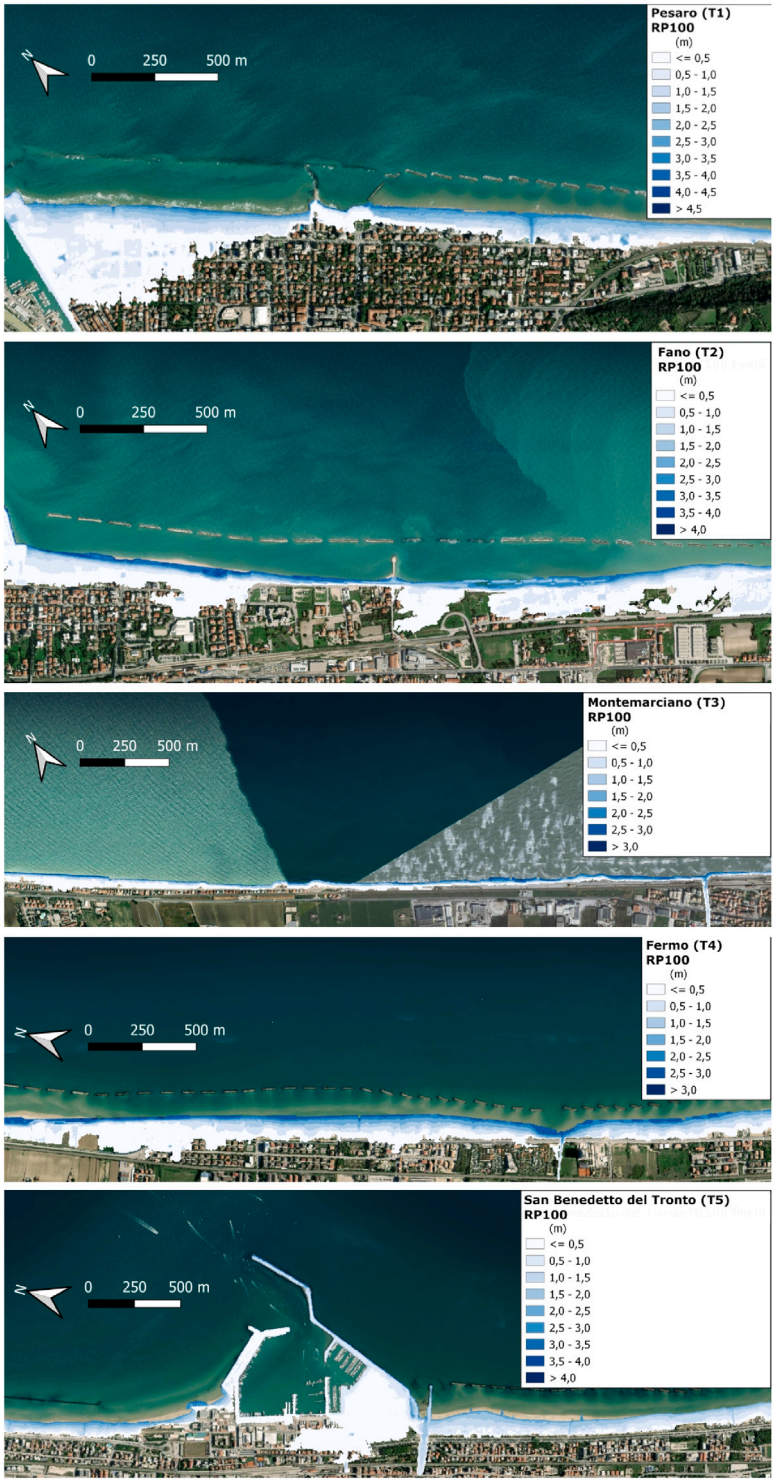

Fig. 8. Inundation maps for the five test sites for the 100-years return period wave storm. Colormaps indicate water depths in the flooded areas. (For interpretation of the references to color in this figure legend, the reader is referred to the web version of this article.)

forces return flows globally equal to the overtopping discharge (Martinelli et al., 2006). Therefore, for a given wave condition, a small piling-up occurs for well emerged conditions, because the overtopping is limited, or for deeply submerged configurations, since the return flow encounters a low resistance. For the same reason, the presence of large gaps between structures also reduces the set-up. On the other hand, the greatest water superelevation verifies for almost null freeboard. Calabrese et al. (2008) developed a method to compute the wave set-up behind submerged structures, based on Dalrymple and Dean (1971), which divides the total set-up into two contributions: the release of momentum flux due to wave breaking, and the generation of a return current needed to compensate for the flux of water mass entering the protected area over the crest of the structure. A number of experimental tests confirmed that, when waves overpass submerged breakwaters, in addition to undergoing a large energy reduction, they also induce a significant water-level increase (Lorenzoni et al., 2016; Martinelli et al., 2006; Calabrese et al., 2008). Lorenzoni et al. (2016) found that the larger is the structure efficiency in terms of wave transmission, the

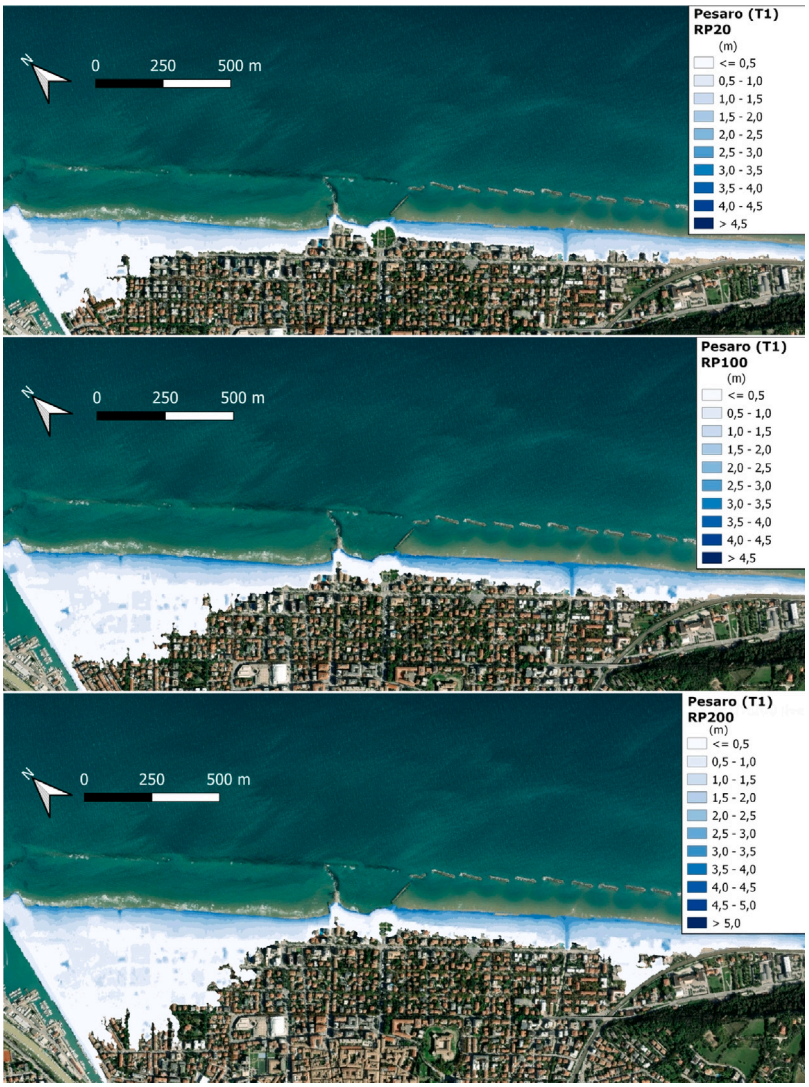

Fig. 9. Inundation maps for Pesaro (T1) and for different return periods (20, 100, 200 years). Colormaps give water depths in the flooded areas. (For interpretation of the references to color in this figure legend, the reader is referred to the web version of this article.)

larger is the piling-up. Therefore, if compared to the emerged breakwaters, submerged structures are less indicated for coastal protection purposes, since the piling-up causes a regression of the shoreline and increases the risk of sea ingression on the land.

This demonstrates that the adaptation of coastal defense structures to CC is not a trivial task and that in-depth evaluations need to be done to choose the most effective intervention depending on expected forcings, such as the wave climate and sea levels, and site-specific conditions, such as the beach profiles and sediment type. Finally, it has been demonstrated that moving the breakwaters closer to shore reduces the beach erosion (Postacchini et al., 2016). However, in terms of beach protection, the major advantages are reached when the structure is moved at a water depth almost equal to the incident wave height, especially for small sea levels (Marini et al., 2020).

4. Conclusions

This study presents a model chain approach to evaluate coastal inundation in a CC scenario projected to 2070. The analysis focuses on five test sites located along the Marche Region coast, in the eastern Mid Adriatic Sea. Numerical solvers are capable of reproducing physical processes not taken into account by simple "bathtub" methods, typically used in the regional planning (Regione Marche, 2019) for the definition of flood risks. Considering phenomena related to wave propagation and dissipation allows one to obtain more reliable inundation perimeters. A further improvement regards the use of a bivariate extreme value analysis to identify the couple H_s-T_p associated to different return periods. Such technique represents a step forward in the identification of extreme forcing values. Instead of performing the extreme value analysis for the wave height and computing the period, through empirical formulations, as a function of the height, here the two variables were jointly evaluated through a copula operator. Results showed that the flooding is more severe in sites characterized by mildly-sloped beaches. However, since the Marche coastal region is highly urbanized, with infrastructures (such as the railway and harbor facilities) and buildings (for residential and touristic/recreational use) located really close to the sea, even a small inland penetration of water leads to major disruptions and damages. Furthermore, the analysis showed that the flood extent increases for increasing return periods. The IPCC (IPCC, 2023) reports with a high confidence level that, due to the rising relative sea level, extreme sea level events that currently occur once in 100 years are projected to become at least annual events in more than half of the considered locations by 2100, under all emission scenarios. In many places, such increase in the frequency of occurrence will even happen in less time, that is, by 2040. Given such projections, it makes sense to observe the specific effect of increasing

Fig. 10. Inundation perimeters for Pesaro (T1) and for different return periods (20, 100, 200 years). Red and green lines represent the perimeters computed by XBeach and that reported in the ICZM Plan. (For interpretation of the references to color in this figure legend, the reader is referred to the web version of this article.)

return periods on coastal inundation maps and to focus on high return periods (low to medium probability of occurrence) scenarios, as we will face extreme events more and more frequently. The comparison of simulated flooding perimeters with the ones reported on the ICZM Plan revealed some differences due to the diverse techniques adopted for their evaluation. Finally, the study showed that particular care needs to be taken in the identification of the best adaptation option for coastal defense structures, because an increase of their elevation does not always lead to flood reduction. The piling-up occurring behind submerged breakwaters, which becomes higher at the increase of the structures' freeboard, causes the worsening of the flood extent and levels, as demonstrated by both the semi-analytical model by Marini et al. (2022) and the numerical results (Fig. 11a and Figure s9 in the Supplementary Material).

CRediT authorship contribution statement

Agnese Baldoni: Methodology, Writing – original draft, Writing – review & editing, Visualization, Conceptualization. **Francesco Marini:** Conceptualization, Methodology, Writing – review & editing, Formal analysis, Writing – original draft. **Giorgio Filomena:** Funding acquisition, Writing – review & editing, Resources, Conceptualization. **Stefano Parlani:** Resources, Conceptualization, Funding acquisition, Writing – review & editing. **Maurizio Brocchini:** Methodology, Conceptualization, Supervision, Writing – review & editing.

Funding sources

This work was funded under the "CoAStal and marine waters integrated monitoring systems for ecosystems proteCtion AnD management" Interreg Italy-Croatia CASCADE project (ID: 10255941).

Declaration of competing interest

The authors declare the following financial interests/personal relationships which may be considered as potential competing interests: Giorgio Filomena reports financial support was provided by European Regional Development Fund. If there are other authors, they declare that they have no known competing financial interests or personal relationships that could have appeared to influence the work reported in this paper.

Appendix A. Supplementary data

Supplementary material related to this article can be found online at https://doi.org/10.1016/j.ecss.2025.109535.

Data availability

Data will be made available on request.

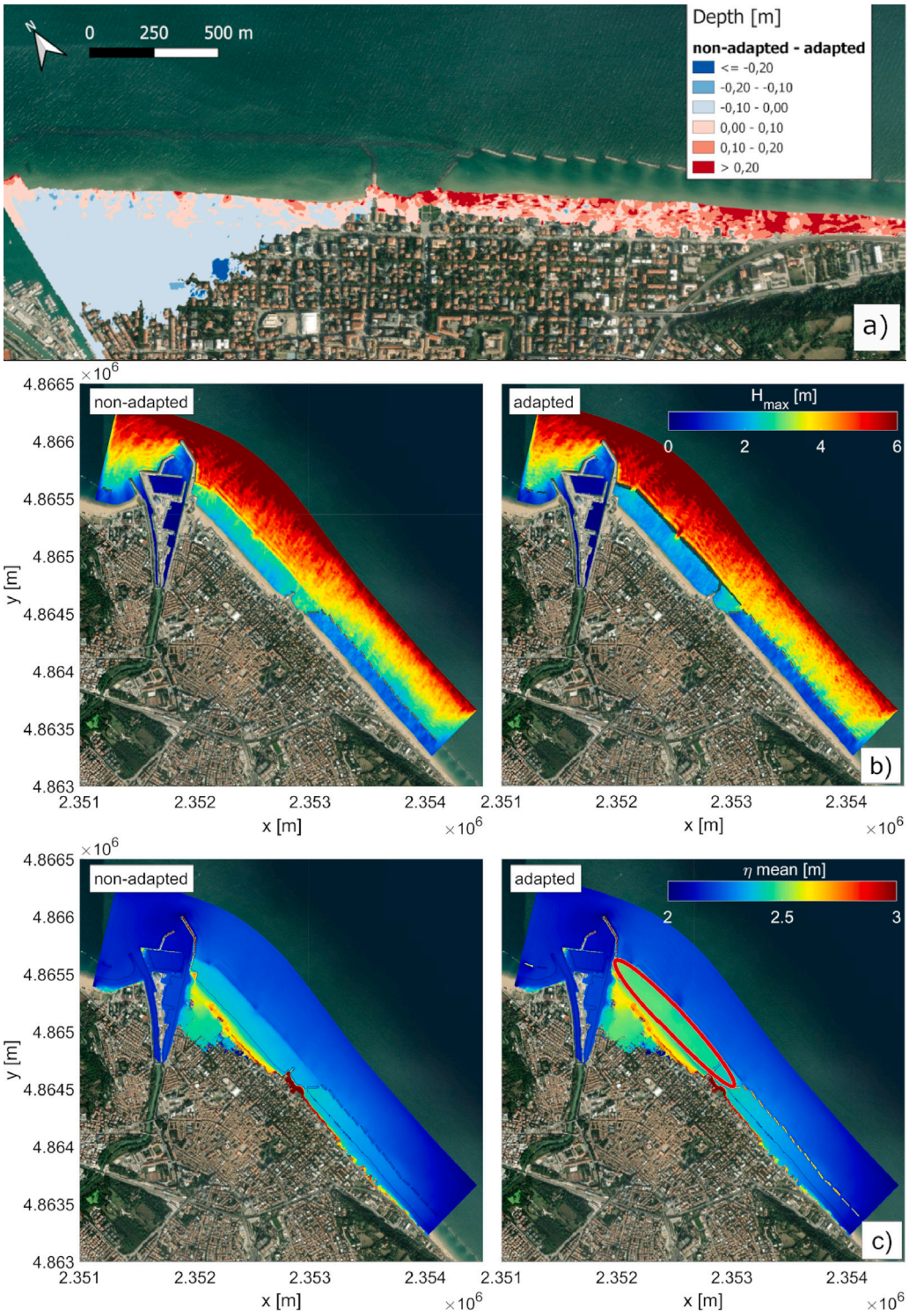

Fig. 11. (a) Differences in water levels between runs with non-adapted and adapted breakwaters; (b) maximum wave height at the sixth hour of the simulation; (c) mean water levels at the sixth hour of the simulation, with a red ellipse highlighting the piling-up effect. (For interpretation of the references to color in this figure legend, the reader is referred to the web version of this article.)

A simple code for shoreline recession (Original data) (Mendeley Data)

References

Amini, E., Marsooli, R., 2023. Multi-scale calibration of a non-hydrostatic model for wave runup simulation. Ocean Eng. 285, 115392. http://dx.doi.org/10.1016/j.oceaneng.2023.115392.

Baldoni, A., Melito, L., Marini, F., Galassi, G., Giacomin, P., Filomena, G., Barbizzi, N., Lorenzoni, C., Brocchini, M., 2024. Modeling coastal inundation for adaptation to climate change at local scale: The case of Marche Region (central Italy). Front. Clim. 6, 1334625. http://dx.doi.org/10.3389/fclim.2024.1334625.

Bates, P.D., Horritt, M.S., Fewtrell, T.J., 2010. A simple inertial formulation of the shallow water equations for efficient two-dimensional flood inundation modelling. J. Hydrol. 387 (1–2), 33–45. http://dx.doi.org/10.1016/j.jhydrol.2010.03.027.

Bertin, X., Bruneau, N., Breilh, J.-F., Fortunato, A.B., Karpytchev, M., 2012. Importance of wave age and resonance in storm surges: The case Xynthia, Bay of Biscay.

Ocean. Model. 42, 16–30. http://dx.doi.org/10.1016/j.ocemod.2011.11.001, URL: https://www.sciencedirect.com/science/article/pii/S1463500311001776.

Bonaldo, D., Antonioli, F., Archetti, R., Bezzi, A., Correggiari, A., Davolio, S., De Falco, G., Fantini, M., Fontolan, G., Furlani, S., et al., 2019. Integrating multidisciplinary instruments for assessing coastal vulnerability to erosion and sea level rise: Lessons and challenges from the Adriatic Sea, Italy. J. Coast. Conserv. 23, 19–37. http://dx.doi.org/10.1007/s11852-018-0633-x.

Bonaldo, D., Bucchignani, E., Pomaro, A., Ricchi, A., Sclavo, M., Carniel, S., 2020. Wind waves in the Adriatic Sea under a severe climate change scenario and implications for the coasts. Int. J. Climatol. 40 (12), 5389–5406. http://dx.doi.org/10.1002/joc.6524.

Bonaldo, D., Bucchignani, E., Ricchi, A., Carniel, S., 2017. Wind storminess in the Adriatic Sea in a climate change scenario. Acta Adriat. 58 (2), 195–208. http://dx.doi.org/10.32582/aa.58.2.1.

Booij, N., Ris, R.C., Holthuijsen, L.H., 1999. A third-generation wave model for coastal regions: 1. Model description and validation. J. Geophys. Res. Ocean. 104 (C4), 7649–7666. http://dx.doi.org/10.1029/98JC02622.

Breilh, J.-F., Chaumillon, E., Bertin, X., Gravelle, M., 2013. Assessment of static flood modeling techniques: Application to contrasting marshes flooded during Xynthia (western France). Nat. Hazards Earth Syst. Sci. 13 (6), 1595–1612. http://dx.doi.org/10.5194/nhess-13-1595-2013.

Caires, S., Yan, K., 2020. Ocean surface wave time series for the European coast from 1976 to 2100 derived from climate projections. Copernic. Clim. Chang. Serv. (C3S) Clim. Data Store (CDS) http://dx.doi.org/10.24381/cds.572bf382, (Accessed 20 January 2023).

Calabrese, M., Vicinanza, D., Buccino, M., 2008. 2D wave setup behind submerged breakwaters. Ocean Eng. 35 (10), 1015–1028. http://dx.doi.org/10.1016/j.oceaneng.2008.03.005.

Christensen, O., Drews, M., Christensen, J., Dethloff, K., Hebestadt, I., Ketelsen, K., Rinke, A., 2007. The HIRHAM Regional Climate Model Version 5 (beta). DMI Technical Report 06-17, Danish Meteorological Institute.

Clarindo, G., Guedes Soares, C., 2024. Environmental contours of sea states by the I-FORM approach derived with the burr-lognormal statistical model. Ocean Eng. 291, 116315. http://dx.doi.org/10.1016/j.oceaneng.2023.116315.

Coblenz, M., 2021. MATVines: A vine copula package for MATLAB. Revstat Stat. J. 14, http://dx.doi.org/10.1016/j.softx.2021.100700.

Coles, S., 2001. An Introduction to Statistical Modeling of Extreme Values. In: Springer Series in Statistics, Springer-Verlag, London.

Corvaro, S., Marini, F., Rocchi, S., Lorenzoni, C., 2025. Extreme storm surge and wave height in the Adriatic Sea. Estuar. Coast. Shelf Sci. submitted for publication.

D'Agostino, R., 1986. Goodness-of-Fit-Techniques, first ed. Routledge, http://dx.doi.org/10.1201/9780203753064.

Dalrymple, R.A., Dean, R.G., 1971. Discussion of "piling-up behind low and submerged permeable breakwaters". J. Waterw. Harb. Coast. Eng. Div. 97 (2), 423–427. http://dx.doi.org/10.1061/AWHCAR.0000093.

Deltares, 2024. Delft3D-WAVE user manual. Simulation of short-crested waves with SWAN. user manual. URL: https://content.oss.deltares.nl/delft3d4/Delft3D-WAVE_User_Manual.pdf.

Den Bieman, J.P., De Ridder, M.P., Doeleman, M.W., 2024. Validation of an efficient non-hydrostatic wave model as a design tool for foreshores in physical models. CoastLab 2024: Phys. Model. Coast. Eng. Sci. http://dx.doi.org/10.59490/coastlab.2024.726.

Dottori, F., Martina, M.L.V., Figueiredo, R., 2018. A methodology for flood susceptibility and vulnerability analysis in complex flood scenarios. J. Flood Risk Manag. 11, S632–S645. http://dx.doi.org/10.1111/jfr3.12234.

Eckert-Gallup, A.C., Sallaberry, C.J., Dallman, A.R., Neary, V.S., 2016. Application of principal component analysis (PCA) and improved joint probability distributions to the inverse first-order reliability method (I-FORM) for predicting extreme sea states. Ocean Eng. 112, 307–319. http://dx.doi.org/10.1016/j.oceaneng.2015.12.018.

ECMWF, 2024. Product User Guide for Sea Level and Ocean Wave Products - Time Series and Indicators. Technical Report, Copernicus Climate Change Service, URL: https://confluence.ecmwf.int/display/CKB/Product+user+guide+for+sea+level+and+ocean+wave+products+-+time+series+and+indicators.

Giorgi, F., 2006. Climate change hot-spots. Geophys. Res. Lett. 33 (8), http://dx.doi.org/10.1029/2006GL025734.

Huang, W., Dong, S., 2021. Joint distribution of significant wave height and zero-up-crossing wave period using mixture copula method. Ocean Eng. 219, 108305. http://dx.doi.org/10.1016/j.oceaneng.2020.108305, URL: https://www.sciencedirect.com/science/article/pii/S0029801820312208.

IPCC, 2023. In: Core Writing Team, Lee, H., Romero, J. (Eds.), Climate Change 2023: Synthesis Report. Contribution of Working Groups I, II and III to the Sixth Assessment Report of the Intergovernmental Panel on Climate Change. Technical Report, IPCC, http://dx.doi.org/10.59327/IPCC/AR6-9789291691647.

Kernkamp, H.W., Van Dam, A., Stelling, G.S., de Goede, E.D., 2011. Efficient scheme for the shallow water equations on unstructured grids with application to the continental shelf. Ocean. Dyn. 61, 1175–1188. http://dx.doi.org/10.1007/s10236-011-0423-6.

Lionello, P., Conte, D., Marzo, L., Scarascia, L., 2017. The contrasting effect of increasing mean sea level and decreasing storminess on the maximum water level during storms along the coast of the Mediterranean Sea in the mid 21st century. Glob. Planet. Change 151, 80–91. http://dx.doi.org/10.1016/j.gloplacha.2016.06.012.

Lorenzoni, C., Postacchini, M., Brocchini, M., Mancinelli, A., 2016. Experimental study of the short-term efficiency of different breakwater configurations on beach protection. J. Ocean. Eng. Mar. Energy 2 (2), 195–210. http://dx.doi.org/10.1007/s40722-016-0051-9.

Marini, F., Corvaro, S., Rocchi, S., Lorenzoni, C., Mancinelli, A., 2022. Semi-analytical model for the evaluation of shoreline recession due to waves and sea level rise. Water 14 (8), 1305. http://dx.doi.org/10.3390/w14081305.

Marini, F., Mancinelli, A., Corvaro, S., Rocchi, S., Lorenzoni, C., 2020. Coastal submerged structures adaptation to sea level rise over different beach profiles. Ital. J. Eng. Geol. Environ. 87–98. http://dx.doi.org/10.4408/IJEGE.2020-01.S-10.

Martinelli, L., Zanuttigh, B., Lamberti, A., 2006. Hydrodynamic and morphodynamic response of isolated and multiple low crested structures: Experiments and simulations. Coast. Eng. 53 (4), 363–379. http://dx.doi.org/10.1016/j.coastaleng.2005.10.018.

Medvedev, I.P., Vilibić, I., Rabinovich, A.B., 2020. Tidal resonance in the Adriatic Sea: Observational evidence. J. Geophys. Res. Ocean. 125 (8), e2020JC016168. http://dx.doi.org/10.1029/2020JC016168.

Mentaschi, L., Vousdoukas, M.I., Voukouvalas, E., Dosio, A., Feyen, L., 2017. Global changes of extreme coastal wave energy fluxes triggered by intensified teleconnection patterns. Geophys. Res. Lett. 44 (5), 2416–2426. http://dx.doi.org/10.1002/2016GL072488, URL: https://agupubs.onlinelibrary.wiley.com/doi/abs/10.1002/2016GL072488. arXiv:https://agupubs.onlinelibrary.wiley.com/doi/pdf/10.1002/2016GL072488.

Mikulić, A., Parunov, J., 2023. Environmental contours in the Adriatic Sea for design and analysis of marine structures. J. Mar. Sci. Eng. 11 (5), http://dx.doi.org/10.3390/jmse11050899.

Montes-Iturrizaga, R., Heredia-Zavoni, E., 2015. Environmental contours using copulas. Appl. Ocean Res. 52, 125–139. http://dx.doi.org/10.1016/j.apor.2015.05.007.

Pasquali, D., Di Risio, M., De Girolamo, P., 2015. A simplified real time method to forecast semi-enclosed basins storm surge. Estuar. Coast. Shelf Sci. 165, 61–69. http://dx.doi.org/10.1016/j.ecss.2015.09.002.

Perini, L., Calabrese, L., Salerno, G., Ciavola, P., Armaroli, C., 2016. Evaluation of coastal vulnerability to flooding: comparison of two different methodologies adopted by the Emilia-Romagna region (Italy). Nat. Hazards Earth Syst. Sci. 16 (1), 181–194. http://dx.doi.org/10.5194/nhess-16-181-2016.

Perini, L., Calabrese, L., Salerno, G., Luciani, P., 2012. Sea-flood hazard mapping in Emilia-Romagna. In: Atti Di: 7th EUREGEO Conference, Bologna. Vol. 1, pp. 334–335. http://dx.doi.org/10.5194/nhess-17-2271-2017.

Postacchini, M., Lalli, F., Memmola, F., Bruschi, A., Bellafiore, D., Lisi, I., Zitti, G., Brocchini, M., 2019. A model chain approach for coastal inundation: Application to the bay of Alghero. Estuar. Coast. Shelf Sci. 219, 56–70. http://dx.doi.org/10.1016/j.ecss.2019.01.013.

Postacchini, M., Russo, A., Carniel, S., Brocchini, M., 2016. Assessing the hydro-morphodynamic response of a beach protected by detached, impermeable, submerged breakwaters: A numerical approach. J. Coast. Res. 32 (3), 590–602. http://dx.doi.org/10.2112/JCOASTRES-D-15-00057.1.

Ragno, E., Antonini, A., Pasquali, D., 2023. Investigating extreme sea level components and their interactions in the Adriatic and Tyrrhenian Seas. Weather. Clim. Extrem. 41, 100590. http://dx.doi.org/10.1016/j.wace.2023.100590.

Regione Marche, 2019. Piano Di Gestione Integrata Delle Zone Costiere (Piano GIZC). Technical Report, Regione Marche. Dipartimento Infrastrutture, Territorio e Protezione Civile. Direzione Ambiente e Risorse Idriche, URL: https://www.regione.marche.it/portals/0/Paesaggio_Territorio_Urbanistica/Difesa_Costa/AggPianoGIZC/Agosto%202022/2022-08-08_PianoGIZCAggLug2022_COMPLETO.pdf.

Ris, R., Holthuijsen, L., Booij, N., 1999. A third-generation wave model for coastal regions: 2. Verification. J. Geophys. Res. Ocean. 104 (C4), 7667–7681. http://dx.doi.org/10.1029/1998JC900123.

Roelvink, D., Reniers, A., Van Dongeren, A., De Vries, J.V.T., McCall, R., Lescinski, J., 2009. Modelling storm impacts on beaches, dunes and barrier islands. Coast. Eng. 56 (11–12), 1133–1152. http://dx.doi.org/10.1016/j.coastaleng.2009.08.006.

Ross, E., Astrup, O.C., Bitner-Gregersen, E., Bunn, N., Feld, G., Gouldby, B., Huseby, A., Liu, Y., Randell, D., Vanem, E., Jonathan, P., 2020. On environmental contours for marine and coastal design. Ocean Eng. 195, 106194. http://dx.doi.org/10.1016/j.oceaneng.2019.106194.

Sanders, B.F., Wing, O.E., Bates, P.D., 2024. Flooding is not like filling a bath. Earth's Futur. 12 (12), e2024EF005164. http://dx.doi.org/10.1029/2024EF005164.

Saranyasoontorn, K., Manuel, L., 2004. Efficient models for wind turbine extreme loads using inverse reliability. J. Wind Eng. Ind. Aerodyn. 92 (10), 789–804. http://dx.doi.org/10.1016/j.jweia.2004.04.002.

Schwab, D.J., Rao, D.B., 1983. Barotropic oscillations of the mediterranean and Adriatic Seas 1. Tellus A 35 (5), 417–427. http://dx.doi.org/10.1111/j.1600-0870.1983.tb00216.x.

Smit, P., Stelling, G., Roelvink, D., van Thiel de Vries, J., McCall, R., Van Dongeren, A., Zwinkels, C., Jacobs, R., 2010. Xbeach: Non-Hydrostatic Model. Validation, Verification and Model Description. Technical Report, Delft University of Technology and Deltares.

Stelling, G., Zijlema, M., 2003. An accurate and efficient finite-difference algorithm for non-hydrostatic free-surface flow with application to wave propagation. Internat. J. Numer. Methods Fluids 43 (1), 1–23. http://dx.doi.org/10.1002/fld.595.

Stockdon, H.F., Holman, R.A., Howd, P.A., Sallenger, Jr., A.H., 2006. Empirical parameterization of setup, swash, and runup. Coast. Eng. 53 (7), 573–588. http://dx.doi.org/10.1016/j.coastaleng.2005.12.005.

Valle-Levinson, A., Marani, M., Carniello, L., D'Alpaos, A., Lanzoni, S., 2021. Astronomic link to anomalously high mean sea level in the northern Adriatic Sea. Estuar. Coast. Shelf Sci. 257, 107418. http://dx.doi.org/10.1016/j.ecss.2021.107418.

Vilibić, I., Šepić, J., Pasarić, M., Orlić, M., 2017. The Adriatic Sea: A long-standing laboratory for sea level studies. Pure Appl. Geophys. 174, 3765–3811. http://dx.doi.org/10.1007/s00024-017-1625-8.

Vousdoukas, M.I., Voukouvalas, E., Annunziato, A., Giardino, A., Feyen, L., 2016a. Projections of extreme storm surge levels along Europe. Clim. Dyn. 47, 3171–3190. http://dx.doi.org/10.1007/s00382-016-3019-5.

Vousdoukas, M.I., Voukouvalas, E., Mentaschi, L., Dottori, F., Giardino, A., Bouziotas, D., Bianchi, A., Salamon, P., Feyen, L., 2016b. Developments in large-scale coastal flood hazard mapping. Nat. Hazards Earth Syst. Sci. 16 (8), 1841–1853. http://dx.doi.org/10.5194/nhess-16-1841-2016.

Winterstein, S.R., Ude, T.C., Cornell, C.A., Bjerager, P., Haver, S., 1993. Environmental parameters for extreme response: Inverse FORM with omission factors. In: Proceedings of the ICOSSAR-93. Innsbruck, Austria, pp. 551–557.

Zebisch, M., Terzi, S., Pittore, M., Renner, K., Schneiderbauer, S., 2022. Climate impact chains—a conceptual modelling approach for climate risk assessment in the context of adaptation planning. In: Climate Adaptation Modelling. Springer International Publishing Cham, pp. 217–224.